RESEARCH ARTICLE

{Macro-
olecular
Materials and Engineering
Open Access
www.mame-journal.de

Improving Infection Resistance in Tissue Engineered Scaffolds for Tensile Applications Using Vancomycin-Embedded Melt Electrowritten Scaffolds

Asha Mathew, Brenna L. Devlin, Dilpreet Singh, Naomi C. Paxton, and Maria A. Woodruff*

It is important to consider mechanical, biological, and antibacterial properties of scaffolds when used for tissue engineering applications. This study presents a method to create complex "wavy" architecture polycaprolactone (PCL) scaffolds toward the development of tissue engineered ligament and tendon tissue substitutes, fabricated using melt electrowriting (MEW) and loaded with vancomycin (5, 10, and 25% w/w). Scaffolds are characterized for both mechanical and biological properties. Loading PCL scaffolds with vancomycin with modified solvent evaporation technique achieves a high loading efficiency of maximum 18% w/w and high encapsulation efficiency with over 89%. Vancomycin loaded PCL scaffolds with all three doses (5, 10, and 25% w/w) display antibacterial activity against Gram-positive *Staphylococcus aureus (S. aureus)* up to 14 days of release. Initial burst followed by a sustained release is observed on all three vancomycin loaded scaffolds for up to 28 days. Importantly, in addition to antibacterial properties, vancomycin-loaded PCL scaffolds also display improved mechanical properties compared to traditional crosshatch design MEW scaffolds and are noncytotoxic at all concentrations as demonstrated by live-dead staining, cell attachment and proliferation assays indicating its potential as an effective treatment option for tissue regeneration in rotator cuff injuries or other tissues undergoing tensile biomechanical loading.

A. Mathew, B. L. Devlin, D. Singh, N. C. Paxton, M. A. Woodruff
Centre for Biomedical Technologies
Queensland University of Technology
60 Musk Avenue, Kelvin Grove 4059, Queensland, Australia
E-mail: mia.woodruff@qut.edu.au
N. C. Paxton
Phil and Penny Knight Campus for Accelerating Scientific Impact
University of Oregon
1505 Franklin Blvd, Eugene 97403, OR, USA

The ORCID identification number(s) for the author(s) of this article can be found under https://doi.org/10.1002/mame.202300168

1. Introduction

Implant-associated infections pose a major challenge in clinical settings, leading to increased morbidity, mortality, and healthcare costs.[1] The development of biomaterials with antimicrobial properties has gained significant attention to overcome this issue.[2] One promising strategy is the use of drug-loaded implants, which can deliver antibiotics directly to the site of infection, or prophylactically release antibiotics locally within a surgical site, resulting in higher local concentrations and lower systemic toxicity. Vancomycin is a commonly used antibiotic for implant-associated infections, due to its broad-spectrum activity against Gram-positive bacteria.[3] However, clinical use of vancomycin is limited by its low systemic absorption, resulting in the need for high doses and potential side effects.[4] Controlled-release systems for localized, sustained delivery to overcome the limitations of conventional antibiotic therapy can improve clinical outcomes in patients with implant-associated infections.

Biofabrication scaffold manufacturing approaches (3D printing) are accelerating the ability to create multifunctional implants that combine the controlled release of bioactive ingredients such as antibiotics while providing a biomechanically relevant scaffolding structure to stabilize a defect region and host tissue regeneration.[5] Of the diverse range of scaffold manufacturing techniques available, melt electrowriting (MEW) is emerging as a promising technique for the fabrication of microfiber scaffolds on a much smaller scale than traditional 3D printing approaches which allow precision control over scaffold architecture[6] and the ability to process a growing number of polymers and polymer composites into suitable scaffolds for tissue engineering applications.[7,8] The process involves melting and extruding a polymer feedstock through a charged nozzle, resulting in the deposition of fibers with diameters ranging from microns to nanometers.[9] MEW scaffolds can mimic the structural and mechanical properties of native tissues, providing an ideal platform for tissue engineering and regenerative medicine applications.[10]

Coupling precision biomimetic scaffold design technology with advanced antibiotic-releasing biomaterials presents a promising new avenue in MEW research. Several recent studies have proposed inclusions of pharmaceutical additives to MEW scaffolds[11] for applications in sublingual drug delivery[12] and the treatment of pelvic organ prolapse (POP).[13] Drug loading, defined as the mass ratio of drug to drug-loaded scaffolds is an important parameter in determining the clinical translation of such scaffolds. Currently, most drug loaded scaffolds have low drug loading of maximum 10% w/w, ranging anywhere between 1 and 10% w/w.[3,12,14,15] Developing high drug loaded scaffolds is still a challenge. Herein, we report for the first time the incorporation of high doses of vancomycin loading (5, 10, and 25% w/w) on MEW scaffolds designed for tensile loading regimes, applicable toward the development of ligament and tendon tissues, among others. Further we characterize the encapsulation efficiency, release profile and antimicrobial activity of vancomycin-embedded MEW scaffolds against common bacterial pathogens responsible for implant-associated infections and biocompatibility in vitro.

The results of this study provide insight into the feasibility and potential of MEW scaffolds as drug delivery systems for mitigating implant-associated infections. This study demonstrates how MEW technology facilitates the design and fabrication of complex structures with tailored mechanics, with high reproducibility and accuracy, opening new avenues for tissue engineering and regenerative medicine applications.

2. Results and Discussion

2.1. Scaffold Fabrication and Mechanical Characterization

A schematic representation of MEW and the use of high voltage, air pressure, and translation speed to deposit fibers on a moving collector is shown in **Figure 1**A. The three scaffold categories investigated are shown in Figure 1B–D, which include two wavy patterns (wavy A and wavy B) with pore size 1250 μm in addition to three different porosities (750, 1000, and 1250 μm) of the well-documented crosshatch scaffold.
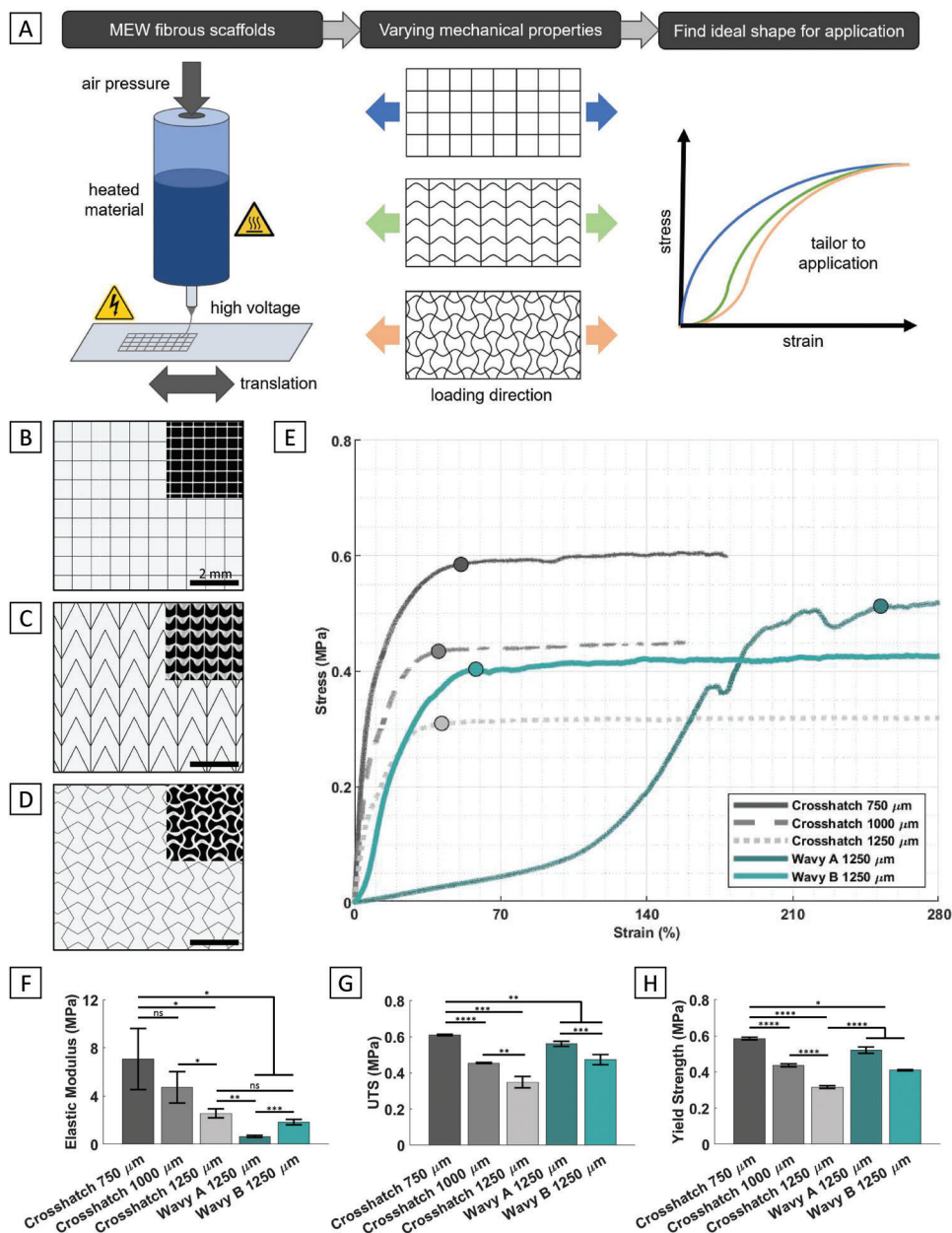
The detailed average mechanical response of different scaffold geometries is shown in Figure 1E and the mechanical properties are listed in **Table 1**. Crosshatch is a simple, model geometry often used as a starting point in tissue-engineered scaffolds due to its rapid fabrication and reproducibility.[16–18] It was observed that the change in pore size of crosshatch scaffolds significantly affected their mechanical properties, such as elastic modulus, ultimate tensile strength (UTS), and yield strength. For example, the reduction in pore size has most pronounced effect on the elastic modulus of scaffolds (Figure 1F), significantly increasing it by ≈86% (1000 μm pore size) and ≈176% (750 μm pore size) compared to 1250 μm pore size, respectively ($p < 0.05$), i.e., from 2.53 ± 0.38 MPa (crosshatch 1250 μm) to 4.73 ± 1.31 MPa (crosshatch 1000 μm), and 7.07 ± 2.53 MPa (crosshatch 750 μm). Whereas UTS and yield strength (Figure 1G,H) observed an increment of ≈30–38% for 1000 μm pore size and ≈75–85% for 750 μm pore size geometry, respectively. This behavior can be attributed to the improved mechanical strength due to increased number of fibres in the scaffolds with reduction in pore size. However, crosshatch geometry is characterized by straight fibers and has

limited movement in the longitudinal and transverse directions, making it less than ideal for mimicking tissues such as tendon and muscle due to rigidity.

By utilizing the precise deposition of microscale fibers achieved using MEW, deviating from these straight-line geometries to target more biomimetic mechanical properties is possible.[19–23] Hence, two different scaffold patterns (wavy A and wavy B) with 1250 μm pore size, having different combinations of movement in the longitudinal and transverse directions were subsequently printed and investigated for their mechanical response and suitability for applications in tissue engineering during tensile loading conditions. From Figure 1E, it is observed that as the geometry shifts from crosshatch to wavy pattern, there is a variation in the mechanical response with appearance of very low-stiffness toe region. This resulted from the flexibility introduced into the scaffold design due to wavy fibers which expand in loading directions. Elastic modulus for wavy A and B scaffolds was calculated from the linear elastic region after toe region. While the stiffness of the scaffolds (elastic modulus) decreased significantly from crosshatch (2.53 ± 0.38 MPa) to wavy A geometry (0.64 ± 0.07 MPa) ($p < 0.01$), the drop is not significant for wavy B geometry (1.84 ± 0.23 MPa). The wavy A geometry has the longest length of fiber to uncrimp during loading (≈2.80 mm of diagonal fibers per 1.25 mm spacing between straight fibers, causing the observed elongated toe region and slower transition to the linear region compared to wavy B geometry that only had a total length of ≈1.50 mm fiber to uncrimp during loading. The larger amplitude of the wavy A fibers resulted in errors due to layer shifting[21,24] which also led to a slight decrease in the elastic modulus (Figure 1F). In contrast, UTS (Figure 1G) and yield strength (Figure 1H) showed a significant increase for both wavy A (>60%) and wavy B (>29%) geometries respectively, indicating superior failure performance of wavy scaffolds. Furthermore, the mechanical response curve of wavy B geometry is similar to the J-shape curve of human supraspinatus tendon studied by Smith et al. and shown in Figure S1 (Supporting Information).[25] While wavy B shows a promising alternative, due to added flexibility, further investigation is needed to fully characterize the scaffold parameters to tune their mechanical properties to mimic human tissue. Hence, it was concluded from the initial mechanical analysis that the wavy B geometry was the most suitable for the rotator cuff application, so this was carried forward for the antimicrobial loading and release studies.

2.2. Mechanical Testing of Geometrically Optimized Vancomycin-Coated MEW Scaffolds

Since this study presents coating of PCL scaffolds with very high doses of vancomycin (5, 10, and 25% w/w), it is important to study their effect on the mechanical properties of scaffolds, especially for load bearing applications. The stress–strain response data of the chosen wavy scaffold geometry with different antimicrobial coating compositions is shown in **Figure 2**A, with elastic modulus, UTS and yield in Figure 2B–D, respectively. These results are also summarized in **Table 2**. Results indicate that vancomycin coating did not significantly affect the mechanical properties of any of the different-coated scaffolds. Although not

ADVANCED SCIENCE NEWS
www.advancedsciencenews.com

acro-
olecular
Materials and Engineering
Open Access
www.mame-journal.de

Figure 1. A) Melt electrowriting (MEW) schematic with mechanical loading direction and response. B–D) Scaffold designs with optical micrograph insert of printed scaffolds with 1250 µm pore size (scale 2 mm). B) Crosshatch, C) wavy A and D) wavy B scaffold geometries respectively. E) Average stress–strain response curves obtained for (a) crosshatch 750 µm, b) crosshatch 1000 µm, c) crosshatch 1250 µm, d) wavy A 1250 µm, and a) wavy B 1250 µm with the yield point denoted by the circle. F–H) Average mechanical properties of different scaffolds including F) elastic modulus, G) UTS, and H) yield strength. ($n=3$, with $^*p \leq 0.05$, $^{**}p < 0.01$, $^{**}p < 0.001$, $^{***}p < 0.0001$, $^{****}p < 0.00001$, and ns = nonsignificant).

significant, elastic modulus increased for all compositions of antimicrobial coating compared to the uncoated control group. However, the UTS and yield strength showed a mixed trend. While the UTS and yield strength of the 5% w/w (5%V-PCL) and 25% w/w (25%V-PCL) groups showed a slight reduction of approximately 0.5% and 2.5%, and ≈3.5%, respectively, with respect to the uncoated scaffold, and a slight increase in UTS and yield strength by almost 3.0% and 3.5% was observed for the 10% w/w (10%V-PCL) group. Overall, the antimicrobial coatings did not adversely affect the PCL scaffolds.

2.3. Vancomycin Loading, Encapsulation and Release from MEW Scaffolds

Antibiotic-loaded scaffolds can be prepared either by mixing antibiotics with polymer solution and solution spinning to form antibiotic encapsulated nanofibers[26] by encapsulating antibiotic loaded microspheres onto scaffolds,[27,28] by incubating scaffolds in antibiotics coagulation bath also known as dip coating[29] or by solvent evaporation techniques.[30] Of the above mentioned methods, encapsulation efficiency has been shown to be highest

ADVANCED
SCIENCE NEWS

www.advancedsciencenews.com

{M} acro-
olecular
Materials and Engineering
Open Access

www.mame-journal.de

Table 1. Average scaffold and mechanical properties of the different geometries (*n*=3).

| Geometry	Elastic modulus [MPa]	UTS [MPa]	Yield strength [MPa]
Crosshatch 750 μm	7.07 ± 2.53	0.61 ± 0.01	0.58 ± 0.01
Crosshatch 1000 μm	4.73 ± 1.31	0.46 ± 0.01	0.44 ± 0.01
Crosshatch 1250 μm	2.53 ± 0.38	0.35 ± 0.03	0.32 ± 0.01
Wavy A 1250 μm	0.64 ± 0.07	0.56 ± 0.01	0.52 ± 0.02
*Wavy B 1250 μm	1.84 ± 0.23	0.47 ± 0.03	0.41 ± 0.01

*Denotes the selected geometry.

Table 2. Average mechanical properties of the shortlisted wavy B scaffold geometry with different antimicrobial coating compositions (*n*=3).

Vancomycin coating	Elastic modulus [MPa]	UTS [MPa]	Yield strength [MPa]
Uncoated (control) PCL	1.84 ± 0.37	0.55 ± 0.01	0.52 ± 0.02
5%V-PCL	2.11 ± 0.19	0.55 ± 0.01	0.49 ± 0.02
10%V-PCL	2.17 ± 0.23	0.57 ± 0.02	0.53 ± 0.01
25%V-PCL	2.11 ± 0.16	0.54 ± 0.02	0.49 ± 0.03

% Variance in properties	Elastic modulus [MPa]	UTS [MPa]	Yield strength [MPa]
Uncoated (control) PCL		Reference values	
5%V-PCL	+14.70	−0.47	−3.36
10%V-PCL	+18.00	+2.98	+3.48
25%V-PCL	+14.72	−2.37	−3.31

using the solvent evaporation technique (>80%).[30] Hence, we employed a modified solvent evaporation technique in this study, to load vancomycin onto the MEW PCL scaffolds using three different doses; 50 μg mg^{-1} (5% w/w), 100 μg mg^{-1} (10% w/w), and 250 μg mg^{-1} (25% w/w). Since, vancomycin is poorly soluble in 100% ethanol, a 50% ethanol was used as the solvent. An amount of 5, 10, and 25% w/w of vancomycin was dissolved in 50% ethanol in which MEW scaffolds were incubated for 8 h to allow ambient time for adhesion. Solvent was completely removed by leaving the scaffolds under hood overnight. A reproducible loading with high encapsulation efficiency was achieved using this technique. As shown in **Figure 3**A, when loaded with 5, 10, and 25% w/w of vancomycin, wavy MEW scaffolds displayed an encapsulation efficiency of 99.09 ± 7.40%, 98.15 ± 2.80%, and 89.91

± 3.60%, respectively. Previous studies reported 1.67% w/w loading efficiency of vancomycin onto PCL coated bioceramic scaffold via dip coating,[31] 5% w/w loading efficiency of nanofibers produced by co-spinning vancomycin with PCL solution,[3] and a maximum 9% w/w loading efficiency of vancomycin-loaded polycaprolactone/polyethylene oxide/hydroxyapatite 3D scaffolds via direct ink writing.[32] A loading efficiency of 18.40% w/w (weight of vancomycin loaded on scaffold/ total weight of the scaffold
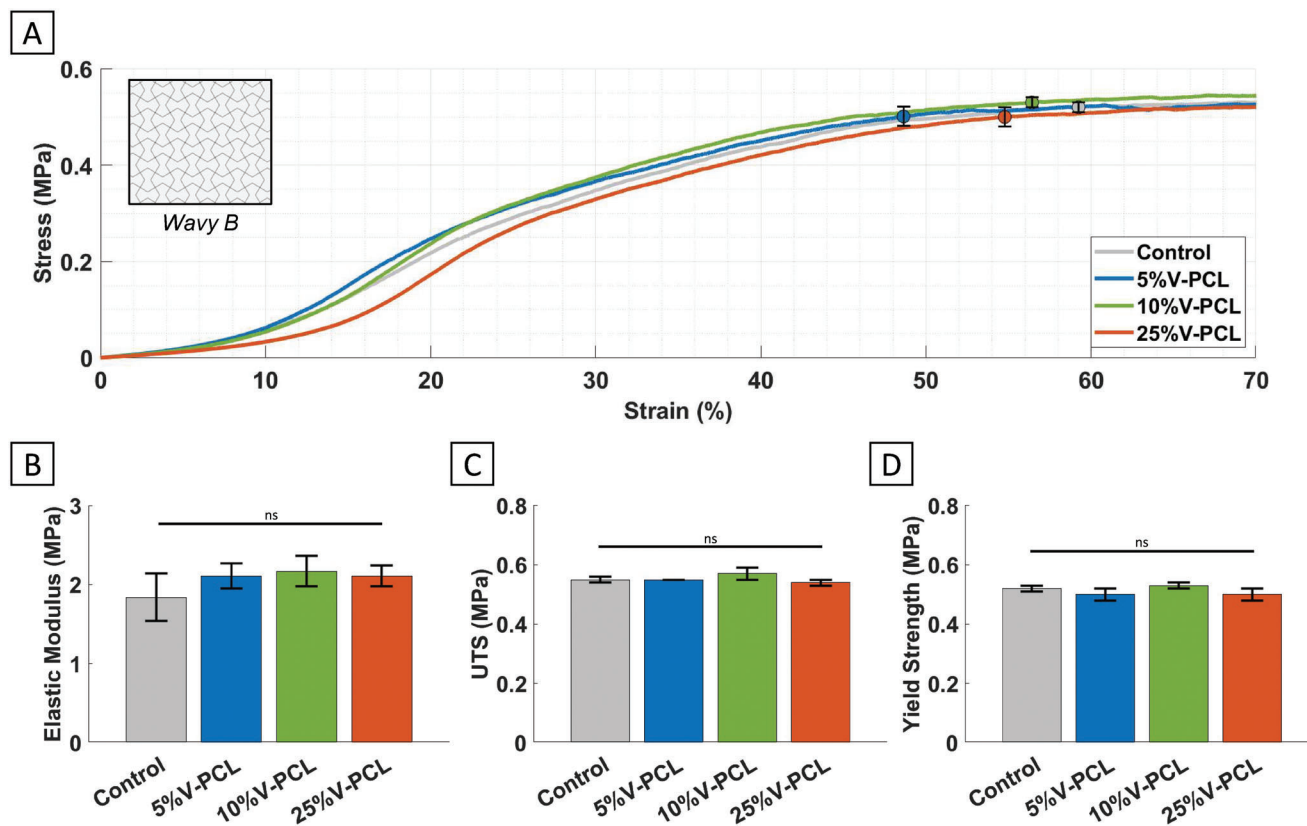
Figure 2. A) The linear elastic stress–strain data for the optimized geometry and each vancomycin concentration, B) the elastic modulus, C) UTS, and D) yield strength. n=3 and ns = no significant difference.
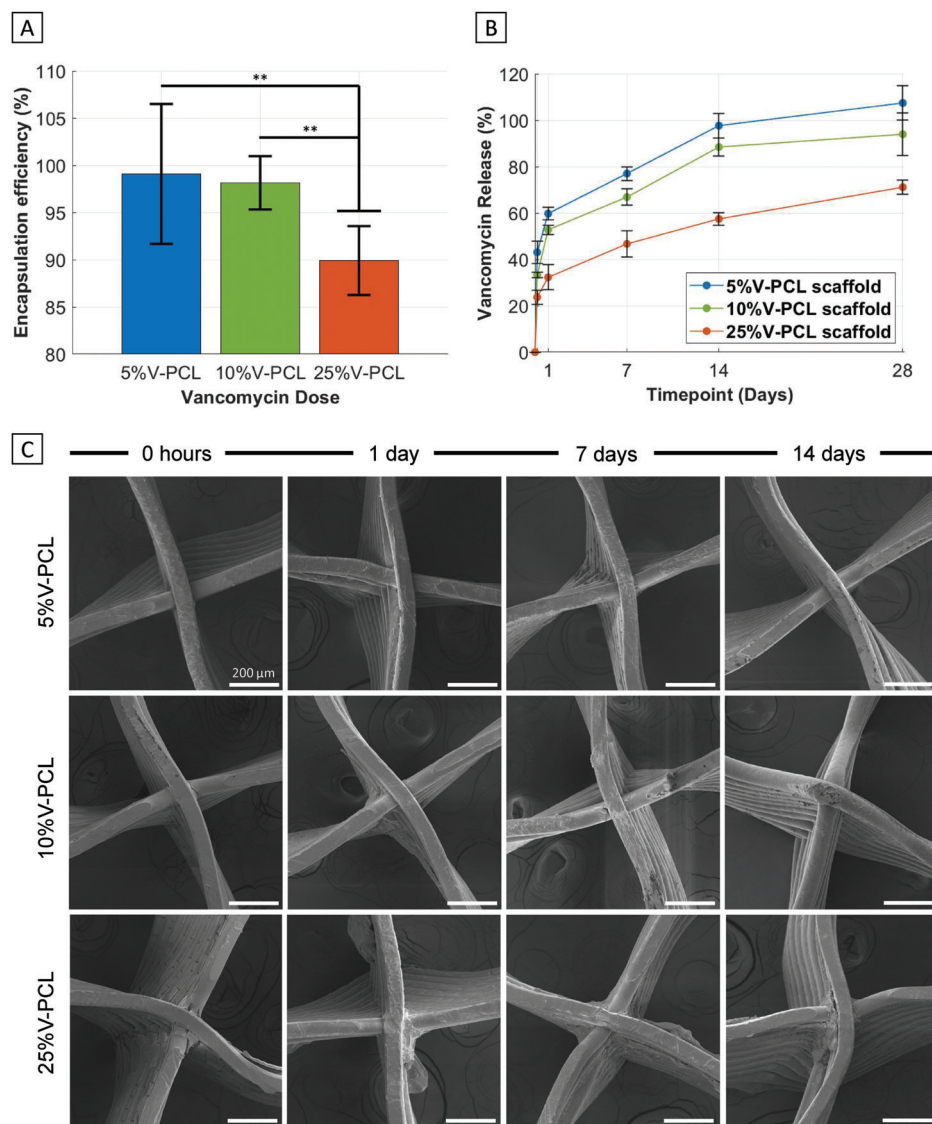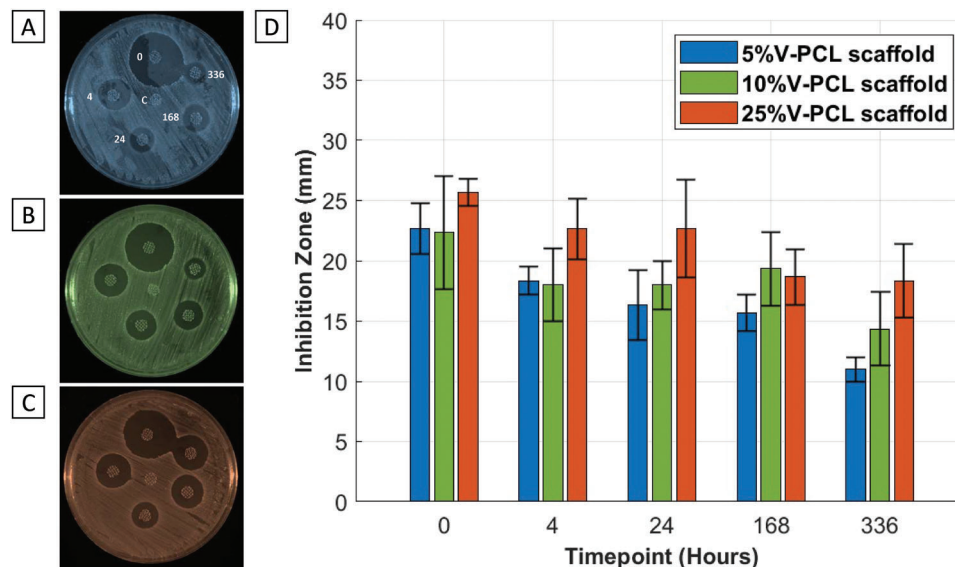
Figure 3. A) Vancomycin encapsulation efficiency and B) release profile of vancomycin loaded on wavy melt electrowriting (MEW) scaffolds. The graph represents the percentage of vancomycin encapsulation and release at various time points from 4 h to 28 days. C) SEM images of vancomycin loaded on wavy MEW scaffolds before and after 1, 7, and 14 days of release in PBS at 37 °C. $n=8$ for both loading and release studies. $^{**}p < 0.001$.

after vancomycin loading) was acheived for 25%V-PCL group which is almost twice the loading efficiency (w/w) compared to other loading techniques reported previously. Scanning electron microscopy (SEM) micrographs show uniform coating of vancomycin onto MEW scaffolds at various doses (Figure 3C). For high doses (25% w/w), a thick coating of vancomycin on to fibers was visible. As shown in Figure 3A, the encapsulation efficiency decreased by increasing the vancomycin loading on MEW scaffolds from 5% to 25%. This indicates that at 25% w/w entire scaffold is coated with vancomycin with no room for further loading which would have resulted in the reduction in loading efficiency from 98.10% to 89.90%. Even at this high loading concentration, encapsulation efficiency is much higher that other previously reported techniques. Previous studies suggest that co-extrusion of nanofibers with antibiotics and in situ coating of antibiotic loaded microspheres has a maximum of 80% encapsulation efficiency

(weight of drug encapsulated on the carrier system/weight of drug added)[26,28] whereas immersion of scaffolds in antibiotic coagulation bath has the least encapsulation efficiency of maximum 30%. Solvent evaporation techniques are most favorable for hydrophobic drugs, however, this method could be also employed for hydrophilic drugs such as vancomycin which we have demonstrated can be dissolved in at least 50% ethanol.

The release kinetics of the vancomycin-loaded MEW scaffolds was investigated in vitro over 28 days. Previous studies have shown that a reversible cellular association happens between bacteria implant surface in the first 1–2 h postimplantation and around 2–3 h postimplantation a strong adhesion resulting in irreversible molecular binding occurs between bacteria and implant surface.[33] Hence, the first 4 h post-implantation are considered critical. Therefore, a burst release of antibiotics in the first few hours of implantation is an important

2300168 (5 of 10)

ADVANCED
SCIENCE NEWS
www.advancedsciencenews.com

{M} macro-molecular
Materials and Engineering
Open Access
www.mame-journal.de

Figure 4. Conservation of the drug bioactivity over 14 days of release in vitro. A–C) *Staphylococcus aureus* agar plate growth inhibition assay for various doses of vancomycin and D) quantification of the growth inhibition for various doses of vancomycin over 0 to 14 days of release in PBS at 37 °C (*n*=3).

requirement for preventing bacterial colonization on the implanted material.

A total of 43.08 ± 4.80%, 33.27 ± 1.14%, and 23.68 ± 3.03% release was observed within 4 h of incubation at 37°C in PBS for 5%V-PCL, 10%V-PCL, and 25%V-PCL, respectively (Figure 3B). With lower doses the release followed a biphasic profile with an initial burst release of vancomycin in the first 0–4 h followed by a more sustained release over the next 28 days. Within 14 days, 97.69 ± 5.30% of vancomycin was released from 5%V-PCL, while the 10%V-PCL group showed 88.45 ± 3.80% release and the 25%V-PCL group released 57.46 ± 2.72% of the drug. By 28 days, 100% drug was released from 5%V-PCL, 93.98 ± 9.07% from 10%V-PCL, and 71.13 ± 3.07% from 25%V-PCL (Figure 3B). The initial dose of vancomycin significantly affected the early and late phases of the release. SEM imaging confirmed the continuous release of vancomycin over the experimental time frame with a gradual exposure of the PCL fibers as the drug was released, as shown in Figure 3C. Traces of vancomycin, as observed by SEM, were still found on scaffolds coated with 10%V-PCL after 7- and 14-days release, while 25%V-PCL shows adhered vancomycin even at 28 day release in PBS at 37°C which supports the release kinetics data shown in Figure 3B. According to previous reports, clinical signs of infection after arthroscopic rotator cuff repair was presented in patients between 7–78 days postsurgery.[34] Hence, sustained release of antibiotics over 1–2 months post-surgery is desirable, suggesting 25%V-PCL group as a potential best choice for clinical application.

2.4. In Vitro Antibacterial Activity of Vancomycin-Loaded Scaffolds on *Staphylococcus Aureus*

Staphylococcus aureus (*S. aureus*) infections are common among implant related infections especially with orthopedic, shoulder, or rotator cuff repair surgeries.[35–37] Hence, the antibacterial efficacy of vancomycin-loaded wavy scaffolds against *S. aureus*

was assessed. The disk diffusion test demonstrated that all three doses of vancomycin on MEW scaffolds were highly able to prevent *S. aureus* proliferation with a distinct zone of inhibition visible around the scaffolds as depicted in **Figure 4**A–C. It is also important for a carrier system to preserve the bioactivity of the antibiotics over the time frame of the drug release. The present study demonstrated that the scaffolds loaded with vancomycin displayed antibacterial activity even after 14 days of release in PBS at 37°C, shown in Figure 4.

2.5. Cell Viability and Proliferation of MSCs on Vancomycin-Loaded MEW Scaffolds

To assess the biocompatibility of MEW scaffolds loaded with high doses of vancomycin, an in vitro study was conducted to assess the behavior of mesenchymal stem cells (MSCs) on vancomycin-loaded MEW scaffolds. Cell nuclei and cytoskeleton were visualized using fluorescence microscopy on days 3 and 7. The hydrophilic nature of vancomycin facilitated an increase in cell attachment on the antibiotic-loaded groups compared to the uncoated control group. By day 7, the cells can be seen to have migrated through the layers of the scaffold, shown in **Figure 5**A. The smallest inter-fiber distance of these wavy scaffolds is still quite large (approximately 300 µm) however the early stages of cell bridging can be seen. Cell viability using a live dead stain also showed high viability on days 1 and 7 for all groups as shown in Figure 5B. Increased cellular metabolic activity was observed in the 5%V-PCL and 10% V-PCL group at different time points based on the alamarBlue results seen in Figure 5C. The 25% V-PCL group showed a considerable decrease in proliferative behavior between days 1 and 7 compared to 5%V-PCL and 10% V-PCL group. This might be due to the higher amount of vancomycin released from 25%V-PCL group days 1 to 7. Approximately 22, 44, and 100 µg of vancomycin was released from 5%V-PCL, 10% V-PCL, and 25%V-PCL group, respectively, between days 1 and
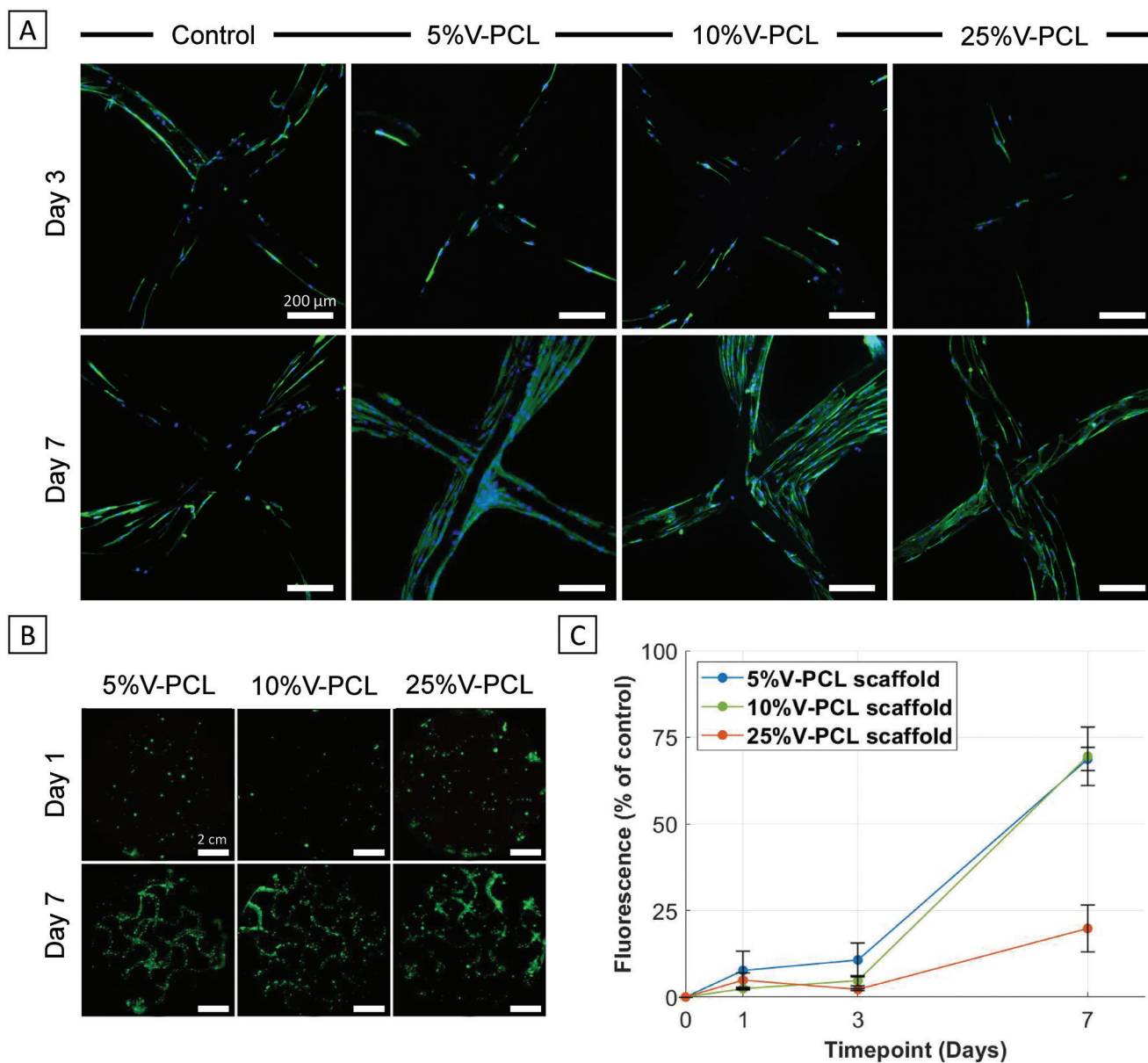
Figure 5. A) Nuclei and cytoskeleton fluorescence microscopy images of mesenchymal stem cells (MSCs) cultured on three doses of vancomycin-loaded scaffolds (5%V-PLC, 10%V-PCL and 25%V-PCL) at days 3 and 7. The control sample refers to a scaffold with no antibiotic coating, B) the live dead cell viability results at days 1 and 7, and C) the cellular metabolic activity measured using the fluorescence emitted at 582 nm for each concentration of vancomycin (n=3).

7. However, it should be noted that in all doses cellular metabolic activity of MSCs was improved when compared to control group with no vancomycin coating. A previous study reported a dose dependent cell death of MSCs when treated directly with various doses of vancomycin.[38] According to this study a direct dose of 40, 160, 320, 640, and 1280 µg induced 9.43%, 13.79%, 19.35%, 24.80%, and 51.85% cell death, respectively, when compared to no vancomycin treatment group. Our results suggest that loading vancomycin onto MEW PCL scaffolds that mimic the structural and mechanical properties of native tissue is creating an ideal environment for cells to attach and proliferate. However,

proliferative behavior of the cells is dependent on the amount of vancomycin released.

3. Conclusion

In the present study, we present a new methodology to embed high doses of vancomycin on MEW PCL scaffolds which can prevent infection without compromising scaffolds mechanical and biological properties. To achieve high antibiotic loading, we employed a simple modified solvent evaporation technique. High antibiotic loading of 18.4% w/w (weight of vancomycin loaded

**ADVANCED
SCIENCE NEWS**

www.advancedsciencenews.com

**Macro-
molecular
Materials and Engineering**
Open Access

www.mame-journal.de

on scaffold/total weight of the scaffold after vancomycin loading) was achieved which is an impressive twofold increase in loading efficiency compared to current coating methods. Encapsulation efficiency ranging from 89% to 99% was achieved by varying the drug dose from 25% to 5%. A burst release followed by a sustained release of vancomycin was observed with all tested doses of vancomycin loaded scaffolds. A prolonged release over 28 days was observed on MEW scaffolds loaded with the highest concentration of vancomycin suggesting its potential to fight infections occurring at the later stages of implantation. High loading of vancomycin on MEW PCL scaffolds did not adversely affect the mechanical properties, cell adhesion, and proliferation, further supporting its potential as an ideal scaffold for tissue engineering and regeneration purposes.

4. Experimental Section

All reagents were obtained from Sigma–Aldrich (Australia), unless otherwise stated. All solvents were of analytical grade and used without purification.

Melt Electrowriting: To fabricate scaffold constructs with micron scale precision to better mimic the mechanics found in soft tissues, scaffolds were designed in MATLAB and printed using a custom-built MEW printer described previously.[39] Three designs were investigated; the standard crosshatch pattern, used as a control and two sinusoidal waves. The waves are herein referred to as wavy A, which features a wave in the longitudinal direction and straight fibers in the trans-verse direction; and wavy B, which features a wave in both directions. Polycaprolactone (45 kDa) was heated to 90 °C and printed using a 21 G needle. A working distance of 2.5 mm, air pressure of 0.025 MPa, and a translation speed of 600 mm min^{-1} was maintained for each print, slightly above the critical translation speed (CTS) of the jet to ensure straight fibers with minimal deviation from the programmed print path. Scaffolds were programmed with an additional 3 mm fiber path extending beyond the scaffold margins (Figure S2, Supporting Information) to ensure sufficient room for the jet to conform to the sharp corners at the edges of the scaffold. Voltage was maintained at 3.5 kV for the crosshatch pattern and adjusted by up to 0.7 kV for the sinusoidal waves to minimize variation in fiber diameter. Samples were printed in triplicate at a constant scaffold size of 24 × 12 mm.

Vancomycin Loading Onto MEW Scaffolds: To facilitate maximum local administration of antibiotics to the surgical site and to avoid adverse effect of high doses of systemic administration, vancomycin hydrochloride was directly coated onto MEW scaffolds by solvent evaporation techniques[30] with slight modification. Briefly, for preparing samples for mechanical testing, MEW scaffolds (2 × 0.5 cm, 10 layers) were placed into 24-well plates, to which 50 µg mg^{-1} scaffold (5% w/w), 100 µg mg^{-1} scaffold (10% w/w), and 250 µg mg^{-1} scaffold (25% w/w) of vancomycin dissolved in 1000 µL of 50% ethanol as a solvent was added and incubated at room temperature for 8 h under mild agitation. The scaffolds were left in a fume hood for the solvent to evaporate. After complete evaporation of the solvent, samples were removed from the 24-well plates and placed on new 24-well plates until mechanical testing was performed. For encapsulation assays, release, disk diffusion, and cell viability studies, 6 mm biopsy punched MEW scaffolds were used and placed individually into a 2 mL polypropylene Eppendorf tube (flat bottom) for the coating procedure. To this 5, 10 and 25% w/w vancomycin dissolved in 200 µL of 50% ethanol (solvent) was added and incubated at room temperature for 8 h under mild agitation. The scaffolds were left in a fume hood for the solvent to evaporate. After complete evaporation of the solvent, vancomycin loaded scaffolds were carefully removed from the Eppendorf tubes and transferred to 96-well plates and stored at −20 °C until use. The empty Eppendorf tubes were retained for encapsulation studies. The final vancomycin loading was determined as the ratio of the mass of vancomycin to the total mass of the

vancomycin loaded scaffold. The morphology MEW scaffolds both with and without the vancomycin coating were characterized by scanning the gold coated samples with a scanning electron microscope at an accelerated voltage of 10 kV (SEM, Jeol JSM-7001F).

Mechanical Testing: Uniaxial tensile strength testing was performed on MEW PCL scaffolds using a Tytron microforce tester with a 10 N load cell (MTS Systems Corporation, USA) at a strain rate of 1 mm s^{-1} and force-displacement data was recorded. Stress and strain analysis was performed using the relations $\sigma = F/A$ and $\epsilon = \Delta L/L_0$, respectively, where F is the normalized axial force, A is the average cross-section area of the scaffold, L_0 is the initial length, and ΔL is the value of the extension of the scaffolds in the loading direction (Figure 1A) calculated from normalized displacement data measured using tensile tester.[6,10,40–42] The cross-sectional area was approximated as a rectangle using the scaffold height (10 layers × average fiber diameter) and printed scaffold width (12 mm), consistent with previous reports of MEW scaffold mechanical methodology.[19,43] The initial length (L_0) of the test samples in the mechanical testing machine was kept uniform during this test, approximately 10 ± 0.1 mm. Table S1 (Supporting Information) shows the average cross-sectional areas of the scaffolds (mean $\pm$ SD) used for calculating stress and strain, measured using a bright-field electron microscope (Axio Imager M2m, Zeiss, Germany). All scaffold geometries were tested in triplicate and mechanically characterized to determine elastic modulus, yield strength, and ultimate tensile strength. The most suitable scaffold geometry was then selected, based on its similarity to ideal J-shape mechanical response of the scaffold geometry to the human supraspinatus tendon, for analysis using the antibacterial coating. Subsequently, the optimal scaffold design was printed in triplicate, coated, and tested using the same loading protocol to study the effect of different coating compositions on the mechanical properties. Uncoated optimal design PCL scaffolds were tested as a control for comparison. Statistical significance between experimental groups was calculated in Microsoft Excel using a two-tailed Student's *t*-test function to calculate *p*-value and one way ANOVA to identify differences between experimental parameters, where $p < 0.05$ was considered significant.

Encapsulation Efficiency and Release Kinetics of Vancomycin from MEW Scaffolds: One of the most important parameters in developing infection resistant biomedical scaffolds is the encapsulation efficiency of the loaded antibiotics, which is the indicator of loading efficiency of the antibiotics on to the scaffolds. Encapsulation efficiency of vancomycin on to MEW scaffolds was determined via absorbance technique.[44] At first, the vancomycin solution standard curve was plotted. A vancomycin stock solution (1000 µg mL^{-1}) was prepared by dissolving 5 mg of vancomycin in 5 mL of distilled water (dH$_2$O). Serial dilutions were prepared from 1000 to 0 µg mL^{-1} each by diluting the initial concentration to half. An amount of 200 µL of each concentration was transferred to a 96-well plate and then scanned using a microplate spectrophotometer (BIO-RAD xMark Spectrophotometer). The absorbance at these solutions at 282 nm was measured to establish the vancomycin solution standard curve. Based on the relationship between the vancomycin standard solution concentration and the corresponding absorbance at 282 nm, a linear equation for the vancomycin standard curve was obtained. Vancomycin encapsulation onto MEW scaffolds was determined using this standard curve. After completion of vancomycin coating process using modified solvent evaporation technique, each vancomycin loaded scaffold ($n=8$) was first removed from the polypropylene Eppendorf tube and transferred to a 96-well plate. To the polypropylene Eppendorf tubes retained after vancomycin coating process, 1000 µL of dH$_2$O was added and vortexed for 30 s to dissolve any uncoated vancomycin left inside Eppendorf tube. From this 200 µL solution was transferred to a 96-well plate and then scanned using a microplate spectrophotometer (BIO-RAD xMark Spectrophotometer) to measure the absorbance at 282 nm. The absorbances obtained were correlated with a standard vancomycin calibration curve ($R^2 = 0.9997$) to determine the amount of uncoated vancomycin. The final amount of vancomycin loaded onto each scaffold was obtained by subtracting the uncoated amount from the initial amount of vancomycin added at the beginning of the coating process. Encapsulation efficiency was determined as the ratio of weight of vancomycin on the scaffold to the weight of the vancomycin added. For the

release of vancomycin from MEW scaffolds, coated scaffolds ($n=8$) with doses of 50 µg mg^{-1} (5% w/w), 100 µg mg^{-1} (10% w/w), and 250 µg mg^{-1} (25% w/w) were placed in a fresh new Eppendorf tube with 1000 µL PBS at 37 °C under agitation of 80 rpm. At each time point (4 h, 1, 7, 14, and 28 days) 250 µL of PBS was removed (stored at −20°C until evaluation) and replenished with equal volume of fresh PBS. The concentration of released vancomycin at each respective time was determined by measuring the absorbance at 282 nm (wavelength) using BIO-RAD xMark Spectrophotometer and correlating it with the standard vancomycin calibration curve (R^2 = 0.9986).

In Vitro Antibacterial Activity: The antibacterial activity of vancomycin coated MEW scaffolds against *S. aureus* (ATCC 25 923), was determined by disc diffusion method. Briefly, the bacterial strain was inoculated onto Brain Heart Infusion Agar (Oxoid) and incubated at 37°C for 24 h. After incubation, isolated bacterial colonies of the stock culture were suspended in sterile saline until the turbidity was compatible with 0.5 Mac Farland. A 100 µL *S. aureus* suspension was spread onto a Mueller-Hinton agar (Oxoid) plate. MEW scaffolds (6 mm) coated with various doses of vancomycin (5, 10, 25% w/w named hereafter as 5%V-PCL, 10%V-PCL, and 25%V-PCL, respectively) and control scaffold with no vancomycin coating in triplicate were placed onto the agar plate and incubated for at 37°C. To qualitatively evaluate the antibacterial efficacy of the vancomycin-coated scaffolds, samples which had been placed in release media (PBS) for 4 h, 1, 7, and 14 days were removed from Eppendorf tubes at each time point and were also tested using the disc diffusion method. All samples were sterilized for 3 h under UV prior to the disk diffusion test. The bacterial growth on the plate was visualized directly, after incubation of the plates at 37°C for 18 h and the diameter of the inhibition zone was measured according to Clinical and Laboratory Standards Institute (CLSI M02-A10) recommendations.

Cell Viability, Proliferation, and Morphology of Cells Grown on Vancomyocin-Coated and Uncoated PCL Scaffolds: Adipose-derived MSC (ATCC) were cultured according to the provider's protocol. Cells were expanded in basal medium (ATCC, PCS-500-030) supplemented with the recommended growth kit (ATCC, PCS-500-040) to form the complete growth medium. MEW scaffolds with (5%V-PCL, 10%V-PCL, and 25%V-PCL) or without vancomycin coating (PCL) were biopsy punched into 6 mm discs, placed in well plates, and sterilized through UV irradiation. At ≈80% confluency, the cells were seeded at a density of 15000 cells per scaffold. The seeded scaffolds were cultured for 7 days, with the cell culture medium changed every 2–3 days. All assays were performed in triplicate unless otherwise stated.

Cellular viability on the MEW scaffolds was assessed by a live and dead cytotoxicity kit (Invitrogen, L3224). PBS solutions of 0.2% calcein-AM, to stain live cells green (excitation/emission ≈494/517 nm), and 0.05% ethidium homodimer-1, to stain dead cells red (excitation/emission ≈528/617 nm), were prepared. Samples were stained for 20 min followed by subsequent washing steps with PBS. The stained samples were imaged using a fluorescence microscope (AxioObserver 7, Carl Zeiss).

Cellular metabolism was assessed using an alamarBlue (Invitrogen, DAL1100) assay. On days 1, 3, and 7, samples were transferred to a fresh well plate and the culture medium replaced with 300 µL of media containing 10% (v/v) alamarBlue solution. After 4 h incubation at 37°C, the scaffolds were removed and the fluorescence of the medium at an excitation wavelength of 560 nm was recorded using a spectrophotometer (ClarioSTAR, BMG Labtech, Germany). Results were normalized to the control (cells seeded at the bottom of the well plate at day 0 with the same seeding concentration).

At selected time points (days 3 and 7), immunostaining for cell nuclei and F-actin cytoskeleton was performed. The samples were rinsed in PBS then fixed for 30 min in 4% paraformaldehyde in PBS, prior to incubation for 5 min with 0.2% Triton-X100 for membrane permeabilization. The samples were then rinsed in PBS and incubated for 30 min in a PBS solution containing 1:1000 DAPI (4,6-diamino-2-phenylindole, Invitrogen, D1306) and 1:250 Phalloidin (Invitrogen, A12379) with excitation/emission values of ≈358/461 nm and ≈495/518 nm, respectively. Imaging was performed on the AxioObserver 7 microscope using the ApoTome 3 (Carl Zeiss) for precise mathematical sectioning.

Supporting Information

Supporting Information is available from the Wiley Online Library or from the author.

Conflict of Interest

The authors declare no conflict of interest.

Data Availability Statement

The data that support the findings of this study are available from the corresponding author upon reasonable request.

[1] M. Haque, J. Mckimm, M. Sartelli, S. Dhingra, F. M. Labricciosa, S. Islam, D. Jahan, T. Nusrat, T. S. Chowdhury, F. Coccolini, K. Iskandar, F. Catena, J. Charan, *Risk Manage. Healthcare Policy* **2020**, *13*, 1765.

[2] P. P. Kalelkar, M. Riddick, A. J. García, *Nat. Rev. Mater.* **2022**, *7*, 39.

[3] Y. Zhao, C. Tian, K. Wu, X. Zhou, K. Feng, Z. Li, Z. Wang, X. Han, *Front. Bioeng. Biotechnol.* **2021**, *9*, 760395.

[4] S. Patel, C. V. Preuss, F. Bernice, *StatPearls [internet]*, StatPearls Publishing, Florida, USA **2022**.

[5] L. Hao, Z. Tianyuan, Y. Zhen, C. Fuyang, W. Jiang, Y. Zineng, D. Zhengang, L. Shuyun, H. Chunxiang, Y. Zhiguo, G. Quanyi, *Biofabrication* **2021**, *14*, 015001.

[6] N. C. Paxton, M. Lanaro, A. Bo, N. Crooks, M. T. Ross, N. Green, K. Tetsworth, M. C. Allenby, Y. Gu, C. S. Wong, S. K. Powell, M. A. Woodruff, *J. Mech. Behav. Biomed. Mater.* **2020**, *105*, 103695.

[7] J. C. Kade, P. D. Dalton, *Adv. Healthcare Mater.* **2021**, *10*, 2001232.

[8] N. C. Paxton, R. Lamont, T. L. Brooks-Richards, M. A. Woodruff, *3D Print. Med.* **2021**, *5*, 10.

[9] T. M. Robinson, D. W. Hutmacher, P. D. Dalton, *Adv. Funct. Mater.* **2019**, *29*, 1904664.

[10] N. T. Saidy, A. Fernández-Colino, B. S. Heidari, R. Kent, M. Vernon, O. Bas, S. Mulderrig, A. Lubig, J. C. Rodríguez-Cabello, B. Doyle, D. W. Hutmacher, E. M. De-Juan-Pardo, P. Mela, *Adv. Funct. Mater.* **2022**, *32*, 2110716.

[11] T. Xu, J. Gu, J. Meng, L. Du, A. Kumar, H. Xu, *J. Mech. Behav. Biomed. Mater.* **2022**, *132*, 105277.

[12] L. Keßler, Z. Mirzaei, J. C. Kade, R. Luxenhofer, *ACS Appl. Polym. Mater.* **2023**, *5*, 913.

[13] J. Ren, R. Murray, C. S. Wong, J. Qin, M. Chen, M. Totsika, A. D. Riddell, A. Warwick, N. Rukin, M. A. Woodruff, *Polymers* **2022**, *14*, 763.

[14] B. Y. L. Chow, A. Baume, P. Lok, J. D. Cao, N. Coleman, A. J. Ruys, P. Boughton, *J. Biomimetics, Biomater., Tissue Eng.* **2012**, *15*, 55.

[15] C. Zhao, W. Liu, M. Zhu, C. Wu, Y. Zhu, *Bioact. Mater.* **2022**, *18*, 383.

[16] S. K. Powell, N. Ristovski, S. Liao, K. A. Blackwood, M. A. Woodruff, K. I. Momot, *3D Print. Addit. Manuf.* **2014**, *1*, 95.

[17] N. Ristovski, N. Bock, S. Liao, S. K. Powell, J. Ren, G. T. S. Kirby, K. A. Blackwood, M. A. Woodruff, *Biointerphases* **2015**, *10*, 011006.

[18] N. Abbasi, A. Abdal-Hay, S. Hamlet, E. Graham, S. Ivanovski, *ACS Biomater. Sci. Eng.* **2019**, *5*, 3448.

[19] N. T. Saidy, F. Wolf, O. Bas, H. Keijdener, D. W. Hutmacher, P. Mela, E. M. De-Juan-Pardo, *Small* **2019**, *15*, 1900873.

[20] H. Chen, D. F. Baptista, G. Criscenti, J. Crispim, H. Fernandes, C. Van Blitterswijk, R. Truckenmüller, L. Moroni, *Nanoscale* **2019**, *11*, 14312.

[21] I. Liashenko, A. Hrynevich, P. D. Dalton, *Adv. Mater.* **2020**, *32*, 2001874.

[22] B. Mirani, S. Mathew, N. Latifi, M. Labrosse, B. Amsden, C. Simmons, **2022**.

[23] H. Wang, W. Ou, H. Zhong, J. He, Z. Wang, N. Cai, X. Chen, Z. Xue, J. Liao, D. Zhan, *Adv. Nano res.* **2022**, *12*, 151.

[24] K. L. O'neill, P. D. Dalton, *Small Methods* **2023**, 2201589.

[25] R. D. J. Smith, N. Zargar, C. P. Brown, N. S. Nagra, S. G. Dakin, S. J. B. Snelling, O. Hakimi, A. Carr, *J. Shoulder Elbow Surg.* **2017**, *26*, 2038.

[26] J.-H. Shim, M.-J. Kim, J. Y. Park, R. G. Pati, Y.-P. Yun, S. E. Kim, H.-R. Song, D.-W. Cho, *Tissue Eng. Regener. Med.* **2015**, *12*, 283.

[27] E. Malikmammadov, T. E. Tanir, A. Kiziltay, V. Hasirci, N. Hasirci, *J. Biomater. Sci., Polym. Ed.* **2018**, *29*, 805.

[28] Z. Zhou, Q. Yao, L. Li, X. Zhang, B. Wei, L. Yuan, L. Wang, *Med. Sci. Monit.* **2018**, *24*, 6934.

[29] D. Puppi, D. Dinucci, C. Bartoli, C. Mota, C. Migone, F. Dini, G. Barsotti, F. Carlucci, F. Chiellini, *J. Bioact. Compat. Polym.* **2011**, *26*, 478.

[30] A. Mathew, C. Vaquette, S. Hashimi, I. Rathnayake, F. Huygens, D. W. Hutmacher, S. Ivanovski, *Adv. Healthcare Mater.* **2017**, *6*.

[31] N. Kamboj, M. A. Rodríguez, R. Rahmani, K. G. Prashanth, I. Hussainova, *Proc. Est. Acad. Sci. U. S. A.* **2019**, *68*, 185.

[32] B. Zhang, A. K. Nguyen, R. J. Narayan, J. Huang, *J. Am. Ceram. Soc.* **2022**, *105*, 1821.

[33] E. M. Hetrick, M. H. Schoenfisch, *Chem. Soc. Rev.* **2006**, *35*, 780.

[34] J. K. Frank, N. Nadiotis, P. R. Heuberer, B. Laky, W. Anderl, L. Pauzenberger, *Arthrosc., Sports Med., Rehabil.* **2020**, *2*, e315.

[35] G. S. Athwal, J. W. Sperling, D. M. Rispoli, R. H. Cofield, *J. Shoulder Elbow Surg.* **2007**, *16*, 306.

[36] A. L. Chen, J. A. Shapiro, A. K. Ahn, J. D. Zuckerman, F. Cuomo, *J. Shoulder Elbow Surg.* **2003**, *12*, 416.

[37] C. W. K. Rosman, J. M. Van Dijl, J. Sjollema, *Crit. Rev. Microbiol.* **2022**, *48*, 624.

[38] S. Chu, N. Chen, A. B. C. Dang, A. C. Kuo, A. B. C. Dang, *Int. J. Spine Surg.* **2017**, *11*, 12.

[39] M. Lanaro, L. Booth, S. K. Powell, M. A. Woodruff, *Electrofluidodynamic Technologies (EFDTs) for Biomaterials and Medical Devices*, Elsevier, Amsterdam, Netherlands **2018**.

[40] L. Pang, N. C. Paxton, J. Ren, F. Liu, H. Zhan, M. A. Woodruff, A. Bo, Y. Gu, *ACS Appl. Mater. Interfaces* **2020**, *12*, 47993.

[41] N. C. Paxton, R. Daley, D. P. Forrestal, M. C. Allenby, M. A. Woodruff, *Mater. Des.* **2020**, *193*, 108787.

[42] A. B. Mccosker, M. E. Snowdon, R. Lamont, M. A. Woodruff, N. C. Paxton, *Adv. Mater. Technol.* **2022**, *7*, 2200259.

[43] Y. Niu, M. Galluzzi, M. Fu, J. Hu, H. Xia, *J Nanobiotechnol.* **2021**, *19*, 349.

[44] T.-H. Tseng, C.-H. Chang, C.-L. Chen, H. Chiang, H.-Y. Hsieh, J.-H. Wang, T.-H. Young, *BMC Musculoskeletal Disord.* **2022**, *23*, 916.